Geophysical Research Letters

RESEARCH LETTER
10.1029/2020GL087261

Key Points:
- Maps of surface density, degree of mantle melting, and crustal thickness are inferred from geochemical and geodetic data
- We find a high correlation between lateral variations in Mercury's crustal thickness and mantle melt production
- The crust is thickest in the ancient high-Mg region

Supporting Information:
- Supporting Information S1

Correspondence to:
M. Beuthe,
mikael.beuthe@observatory.be

Citation:
Beuthe, M., Charlier, B., Namur, O., Rivoldini, A., & Van Hoolst, T. (2020). Mercury's crustal thickness correlates with lateral variations in mantle melt production. *Geophysical Research Letters*, *47*, e2020GL087261. https://doi.org/10.1029/2020GL087261

Received 27 JAN 2020
Accepted 6 APR 2020
Accepted article online 17 APR 2020

Mercury's Crustal Thickness Correlates With Lateral Variations in Mantle Melt Production

Mikael Beuthe[1], Bernard Charlier[2], Olivier Namur[3], Attilio Rivoldini[1], and Tim Van Hoolst[1,4]

[1]Royal Observatory of Belgium, Brussels, Belgium, [2]Department of Geology, University of Liège, Sart Tilman, Belgium, [3]Department of Earth and Environmental Sciences, KU Leuven, Leuven, Belgium, [4]Institute of Astronomy, KU Leuven, Leuven, Belgium

Abstract Over the first billion years of Mercury's history, mantle melting and surface volcanism produced a secondary magmatic crust varying spatially in composition and mineralogy. By combining geochemical mapping from MESSENGER with laboratory experiments on partial melting, we translate the surface mineralogy into lateral variations of surface density and calculate the degree of mantle melting required to produce surface rocks. If lateral density variations extend through the whole crust, the local crustal thickness correlates well with the degree of mantle melting. Low-degree mantle melting produced a thin crust below the northern volcanic plains (19 ± 3 km), whereas high-degree melting produced the thickest crust in the ancient high-Mg region (50 ± 12 km), refuting the hypothesis of an impact origin for that region. The thickness-melting correlation has also been observed for the oceanic crust on Earth and might be a common feature of secondary crust formation on terrestrial planets.

Plain Language Summary Mercury's crust has a complex structure resulting from a billion years of volcanism. The surface variations in chemical composition have been identified from orbit by the spacecraft MESSENGER. Combining these measurements with laboratory experiments on partial melting, we estimate which variations in surface density and degree of mantle melting are required to produce surface rocks. If the surface density is representative of the deep crustal density, more than one half of crustal thickness variations in the Northern Hemisphere are explained by lateral variations in mantle melting. The crust is thin below the magnesium-poor northern volcanic plains, whereas the thickest crust is found in the magnesium-rich region located at middle northern latitudes in the Western Hemisphere. The magnesium-rich region is thus not due to an early impact but rather to extensive mantle melting. The thickness-melting relation has also been observed for the oceanic crust on Earth and might be a common feature of terrestrial planets.

1. Introduction

The surface of Mercury is mainly composed of lavas (Head et al., 2008). Major magmatic activity terminated about 3.5 Ga ago (Byrne et al., 2016; Marchi et al., 2013), so the lavas provide a record of the early stages of the thermal and compositional evolution of the planet (Michel et al., 2013; Padovan et al., 2017; Tosi et al., 2013) and can be used to constrain melting conditions of the mantle (Malavergne et al., 2010; Namur et al., 2016). The volcanic crust of Mercury is made up of several geological units with different ages and compositions (Weider et al., 2015). Smooth plains represent the youngest units and cover about 27% of the surface (Denevi et al., 2013). They contain the northern volcanic plains (NVP), which represent the largest area of flood basalts on Mercury and possibly in the solar system (Head et al., 2011). Recent estimates of the average thickness of Mercury's crust range from 20 to 50 km (Genova et al., 2019; James et al., 2015; Konopliv et al., 2020; Mazarico et al., 2014; Padovan et al., 2015; Phillips et al., 2018; Sori, 2018), and the mantle is 400 km thick (Hauck et al., 2013; Margot et al., 2018; Rivoldini & Van Hoolst, 2013). The crust therefore accounts for between 6% and 16% of the bulk silicate content, suggesting that crustal production is as high or higher than on other terrestrial planets (Padovan et al., 2015; Tosi & Padovan, 2020). In this study we combine the most recent geochemical surface measurements, used to derive crustal density and estimates of degrees of mantle melting, with gravity and topography data obtained by the Mercury Surface, Space Environment, Geochemistry, and Ranging (MESSENGER) spacecraft. In the Northern Hemisphere,

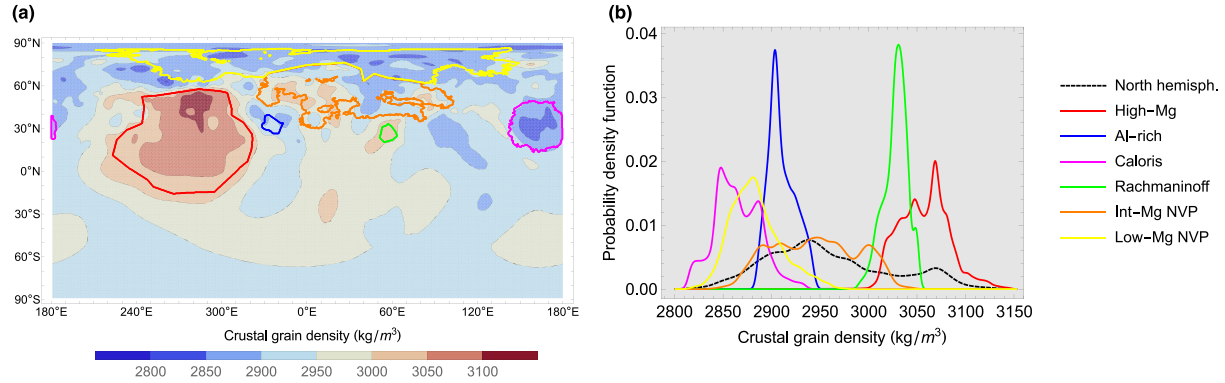

Figure 1. (a) Density of pore-free surface rocks obtained from global mineralogical mapping using MESSENGER XRS measurements for major elements (equirectangular projection). Color lines delimitate geochemical terranes (Weider et al., 2015). (b) Histogram (equal area) of crustal grain density for the North Hemisphere and the geochemical terranes.

where the resolution of MESSENGER geochemical and geophysical data is the highest, we identify a clear relation between geochemical units, crustal thickness, and mantle melt production.

2. Methods

2.1. Crustal Density

Six geochemical terranes were identified on Mercury on the basis of their Al/Si and Mg/Si ratios (Weider et al., 2015): the high-Mg region located in the Western Hemisphere at middle northern latitudes (about 11% of the surface), the low-Mg NVP and Int-Mg NVP (intermediate in their Mg content) making up the NVP (about 7% of the surface), the Rachmaninoff and Caloris basins (about 2% of the surface), and the small Al-rich smooth plains. These terranes make up less than half of the North Hemisphere; the remaining surface is not identified with specific sets of geochemical characteristics. Compositional variations across geochemical terranes reflect different mineralogical assemblages of surface rocks (Namur & Charlier, 2017; Stockstill-Cahill et al., 2012; Vander Kaaden et al., 2017). Crystallization experiments on synthetic samples representative of the geochemical provinces of Mercury and mass balance calculations provide the overall distribution of surface minerals (Namur & Charlier, 2017). Variable mineral proportions translate into pore-free crustal densities at the surface between 2,785 and 3,149 kg/m^3, with an average of 2,957 kg/m^3 (Figure 1; Text S1 and Figure S2). This range is consistent with crustal densities previously calculated from a limited number of normative mineralogy calculations (Sori, 2018); high-resolution gravity data might provide other constraints in the future (James et al., 2019). The largest crustal densities (3,000 to 3,150 kg/m^3) are found in the olivine-rich and plagioclase-poor high-Mg region. The crust is the least dense (2,800 to 2,950 kg/m^3) in the Al-rich/Mg-poor regions such as the NVP, which are plagioclase dominated. The Int-Mg NVP, which contain a higher proportion of olivine and pyroxene compared to low-Mg NVP, have intermediate density values (2,850 to 3,050 kg/m^3). If the crust is porous as on the Moon (Wieczorek et al., 2013) and on Mars (Goossens et al., 2017), the actual crustal density is lower than what the pore-free mineralogy tells us. We thus adopt a compaction model with porosity decreasing exponentially with increasing depth to relate the crustal density to the surface rock density (Besserer et al., 2014; Han et al., 2014) (Text S2). In addition, the density of rocks deeper in the crust may not vary laterally in the same way as surface rocks because magmatic flows and intrusions are not purely radial at small scale. In particular, it is unlikely that the highest and lowest density regions extend as straight columns from the surface down to the mantle-crust boundary. We therefore smooth out lateral density variations with increasing depth (Text S3 and Figure S3).

2.2. Crustal Thickness

The construction of a global map of crustal thickness relies on the inversion of free-air gravity anomalies, which are the result of surface topography, relief at the mantle-crust boundary, and lateral variations in crustal and mantle densities. For lack of high-resolution gravity data or seismic data, crustal and mantle densities are usually supposed to be laterally uniform so that gravity anomalies arise exclusively from undulations of crustal boundaries (previous work is reviewed in Text S4). The most recent crustal thickness map for Mercury based on those assumptions has been computed from the gravity field HgM008 (Genova et al., 2019) and shape model GTMES 150v05 (Neumann et al., 2016), which are given as spherical harmonic

expansions up to degree and order 100 and 150, respectively (the spatial resolution is thus limited by the gravity field). Here we compute a map of lateral variations in crustal thickness that takes into account lateral variations in crustal density and assess the differences with respect to a uniform density model, similarly to what has been done for the Moon (Wieczorek et al., 2013) and for Mars (Goossens et al., 2017). The free parameters of the model are the mantle density, surface porosity, compaction scale depth (specified by the e-folding depth), and the average crustal thickness or, alternatively, the minimum crustal thickness (Text S5). The model also depends on the filtering degree, which parameterizes the suppression of short-wavelength gravity noise at the crust-mantle interface. For the average crustal thickness, we adopt a default value of 35 km to facilitate comparison with previous work, but we also consider models with average thickness of 25 and 45 km, compatible with positive crust thickness everywhere. The assumption that the surface density represents (or not) the density at depth is analyzed with the following models: a first one without smoothing, a second one with more smoothing, a third one with a laterally homogeneous lower crust below 20 km, and a fourth one for which the crustal density in the NVP is taken to be equal to the average surface density (2,957 kg/m^3) in case the lava flows are of limited thickness compared to the total crustal thickness. Crustal thickness could also depend on lateral variations in mantle density. Laboratory experiments indicate that Mercury's residual mantle is mainly made up of two materials with similar densities (Figure S4): olivine (forsterite) and orthopyroxene (enstatite) (Namur et al., 2016). We neglect these lateral variations and set the mantle density at the crust-mantle boundary to a uniform value of $\rho_m = 3,200$ kg/m^3. This assumption could introduce errors of the order of several kilometers on the relief of the crust-mantle boundary if mantle mass anomalies are present (James et al., 2015). We also investigate a case in which degrees 2 and 4 of the gravity and topography arise from thermal perturbations in the mantle due to uneven solar insolation (Tosi et al., 2015). This scenario requires a lithospheric thickness of more than 110 km and therefore a late capture in the 3:2 spin orbit.

2.3. Mantle Melt Production

We calculate the degree of partial melting required to produce the observed lavas at Mercury's surface in areas for which MESSENGER X-ray spectrometer measured the abundance of all major elements (Ca/Si, Mg/Si, Al/Si, Na/Si, and S/Si) (Nittler et al., 2020; Weider et al., 2015). The variable major element chemistry—in particular sodium—of the lavas implies that the mantle must be slightly heterogeneous in composition, with Mg-poor lavas originating from mantle sources with lower CaO and higher Na_2O concentrations than Mg-rich lavas (Namur et al., 2016; Nittler et al., 2018). The two proposed mantle compositions contain similar amounts of Si, Al, and Mg. They significantly differ in Ca and Na content, but the two last components do not exceed 4 to 5 wt.% in total (table 2.2 Nittler et al., 2018). As the effects of CaO and Na_2O on the position of the solidus (and presumably liquidus) approximately cancel out, both mantle sources have similar relations between melting fraction and temperature (Hirschmann, 2000; Wasylenki et al., 2003). Therefore, we assume a homogeneous lherzolitic mantle (olivine and pyroxenes-bearing rock) and calculate mantle melt production using melt isopleths between the liquidus of the silicate fraction of an enstatite chondrite and the solidus of the CaO-MgO-Al_2O_3-SiO_2-Na_2O system (see further discussion in Text S7). Based on these results, we derive an equation giving the melting degree as a function of the two ratios for which complete mapping is available, that is, Mg/Si and Al/Si (Figure S1).

3. Results

Crustal density variations have a significant effect on estimates of local crustal thickness (Figure 2; Table 1; Figure S5). The total range of thickness variability is 60% larger in our new reference model with nonuniform crustal density (8–97 km in our new reference Model V0; Figures 2c and 2d) than without (11–67 km in Model U0 with uniform crustal density; Figures 2a and 2b). The most remarkable difference is that the high-Mg region, which has previously been interpreted as a region of thin crust, turns out to be the area with the thickest crust when crustal density variability is considered (50 ± 11 km; Figures 2c and 2d). The local thickening of the crust compensates the effect of the higher density on gravity. This phenomenon is particularly strong in the highest density patch (25–35° N, 280–300° E). The high-Mg region is therefore not an outcrop of the mantle exhumed by a large impact (Weider et al., 2015) but is rather the result of a high degree of mantle melting (Frank et al., 2017; Namur & Charlier, 2017; Padovan et al., 2017). The crust is much thinner below the NVP (19 ± 3 km in the low-Mg NVP and 25 ± 7 km in the Int-Mg NVP for Model V0). The thinnest crust is beneath the impact-related Caloris basin (7.8 km for Model V0), whereas it is relatively thicker below the Rachmaninoff basin although the basin still corresponds to a local minimum of crustal

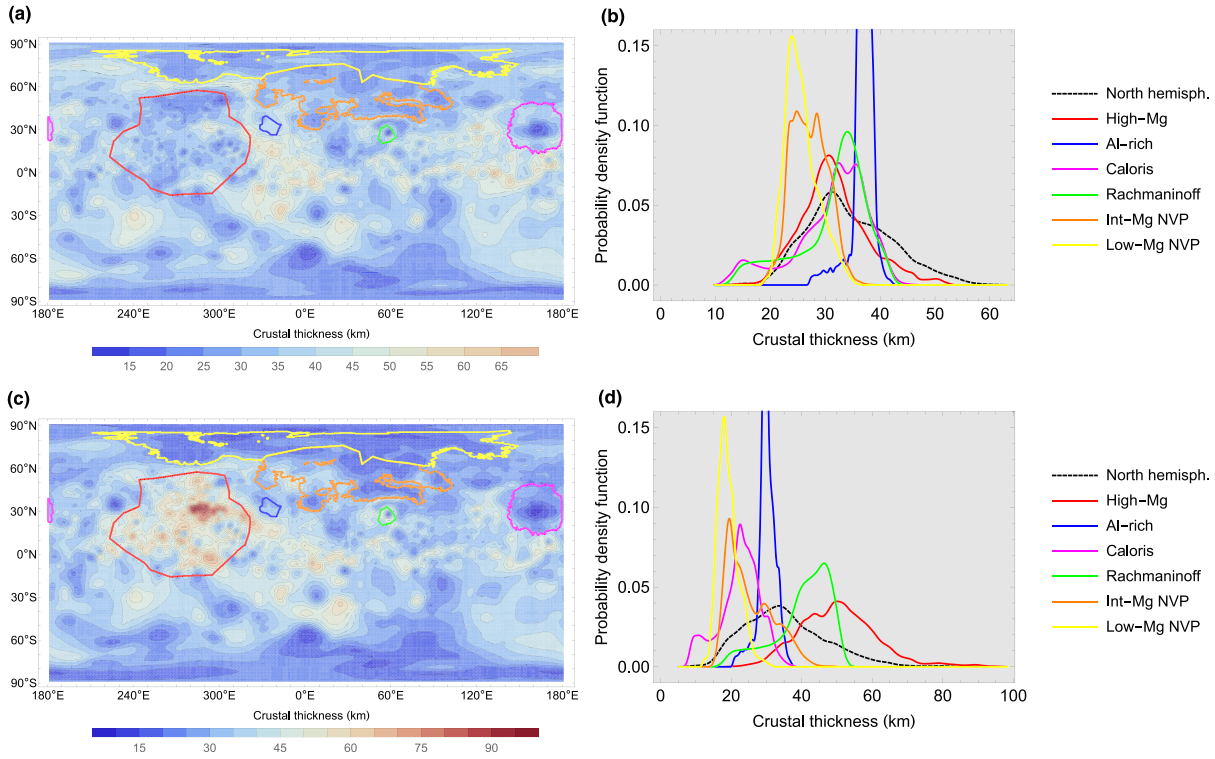

Figure 2. (a) Crustal thickness map if laterally uniform density (Model U0). (b) Histogram of the crustal thickness in the North Hemisphere for Model U0. (c) Crustal thickness map if laterally uniform density (Model V0). (d) Histogram of the crustal thickness in the North Hemisphere for Model V0. The average crustal thickness is 35 km in both models. Map projection is equirectangular. Color lines delimitate geochemical terranes. The color scale is the same in both maps.

thickness. Crustal thickness calculations for different model assumptions confirm the robustness of those results (Table 1 and Text S6).

The correspondence between high-Mg concentrations and thick crust suggests a correlation between the local crustal thickness and the local degree of mantle melting; that is, the higher the degree of melting, the thicker the crust. In agreement with previous calculations based on fewer chemical analyses but including a larger set of chemical elements, we estimate that Mercury's surface lavas were produced by 15% to 50% partial melting of a lherzolitic mantle source (Charlier et al., 2013; Namur et al., 2016). Figure S1 shows the lateral variations in partial melting of the mantle required to produce those lavas. The average melting degree is lower for the low-Mg NVP ($25 \pm 3\%$) with thin crust than for the thick high-Mg terranes ($43 \pm 3\%$). It ranges from 25% to 40% for the compositionally intermediate regions, which also have intermediate crustal thicknesses in models with variable crustal density. This further demonstrates that the high-Mg region is not an outcrop of the mantle but formed as a consequence of the highest degree of partial melting in Mercury's mantle, which led to the intrusion and eruption of Mg-rich lavas and the formation of a thick crust.

In order to quantify the statistical significance of the correlation between crustal thickness and the fraction of melt produced in the mantle, we compute the average crustal thickness and the 95% confidence levels for melt fraction bins of equal width (Figure 3). We find that crustal thickening is strongly correlated with mantle melt fraction but only if lateral variations in crustal density are taken into account (Table 1). In reference Model V0 (variable crustal density), the bin-averaged crustal thickness increases linearly with the bin-averaged melt fraction, with a linear correlation coefficient $r = 0.73$. The coefficient of determination (r^2) indicates that 53% of the crustal thickness variance can be explained by a linear dependence on the melt fraction in Model V0. The slope and correlation between crustal thickness and mantle melt fraction depend on the values of the free parameters of the model. Lowering porosity at the surface (Model V1; $r = 0.68$) or within the crust (Model V2; $r = 0.74$) has little influence on the correlation coefficient. Lowering the average crustal thickness to 25 km (Model V3; $r = 0.57$) or removing the degrees 2 and 4 (Model V5; $r = 0.63$) significantly decreases the correlation, whereas a higher value for the average crustal thickness increases

Table 1
Characteristics of Crustal Thickness Models: Input Parameters, Crustal Thickness Range, and Linear Correlation Coefficient r Between Crustal Thickness and Degree of Mantle Melting

		Input parameters[b]						Crustal thickness		
		$\ell_{1/2}$	ϕ_s	d_ϕ	d_c	d_s	n_0	Min	Max	Correlation
Model[a]	Special feature	(-)	(%)	(km)	(km)	(km)	(-)	(km)	(km)	r
U0	Default if uniform density	40	24	8	35	35	20	11.2	67.2	−0.15
V0	Default if variable density	40	24	8	35	35	20	7.8	97.2	0.73
V1	Lower surface porosity	40	12	8	35	35	20	6.4	103.0	0.68
V2	Less porous at depth	40	24	4	35	35	20	6.8	104.5	0.74
V3	Thin crust	40	24	8	25	25	20	3.3	62.4	0.57
V4	Thick crust	40	24	8	45	45	20	12.9	132.3	0.80
V5	No degrees 2 and 4	40	24	8	35	35	20	6.5	89.2	0.63
V6	No smoothing	40	24	8	35	0	-	7.6	119.9	0.73
V7	More smoothing	40	24	8	35	35	0	−0.7	67.6	0.66
V8	Homogeneous lower crust	40	24	8	35	20	0	4.4	65.9	0.39
V9	NVP of average density	40	24	8	35	35	20	7.7	96.8	0.71
V10	Higher filtering degree	60	24	8	35	35	20	1.5	119.3	0.68

[a] In all models: mantle density = 3,200 kg/m^3; average crustal grain density = 2,957 kg/m^3; $l_{cut} = 100$ (Text S5). [b] $\ell_{1/2}$ = filtering degree; ϕ_s = surface porosity; d_ϕ = compaction e-folding depth; d_c = average crustal thickness; d_s = maximum smoothing depth; n_0 = cutoff degree for smoothing (Text S5).

the correlation (Model V4; $r = 0.80$). Dispensing with smoothing at depth of lateral density variations (Model V6; $r = 0.73$) and assuming that the NVP are of average crustal density (Model V9; $r = 0.71$) have no effect on the correlation. Increasing smoothing at depth (Model V7; $r = 0.66$) and increasing the filtering degree (Model V10; $r = 0.68$) slightly decrease the correlation although it remains significant. The assumption that the crust is homogeneous below a depth of 20 km (Model V8; $r = 0.39$) results in crustal thickness variations much closer to those obtained in the model without lateral density variations so that the correlation between crustal thickness and mantle melt fraction becomes low. A statistical analysis in the spectral domain also shows that the linear relation between crustal thickness and melt fraction is statistically significant at the longest wavelengths ($\lambda \geq 1,400$ km) for the various models considered here (Text S8; Figures S11 and S12).

Two other issues are worth considering. First, could correlation be biased by crust removal due to large impacts? The answer is negative: Excluding large basins (Table 1 Fassett et al., 2012) has a negligible effect on the correlation unless it is already low (column r' in Table S1). Second, correlation could be biased if lavas erupted at a late stage in the NVP because the crust was already thin in that region. Computing the correlation without the NVP, however, barely changes the results for the models with high correlation (column r'' in Table S1).

4. Discussion

A simple scenario of heterogeneous mantle melting followed by melt extraction and secondary crust production thus explains at least 50% of the crustal thickness variability. High degrees of mantle melting produced a large volume of Mg-rich lavas that accumulated to produce a thick crust. Conversely, Mg-poorer lavas were produced by a lower degree of partial mantle melting and formed a thinner crust. Although the degree of partial melting necessary to produce NVP lavas (25 ± 3%) is in the lower range for Mercury, it is relatively high as compared to most lavas produced on Earth (MORB) and is fully consistent with emplacement via flood-style volcanism. For example, the melt fraction inferred for Earth's large igneous provinces peaks at 0.25–0.30 (Herzberg & Gazel, 2009).

The production of localized thickened crustal units on Mercury might have several origins. A main mechanism of partial melting of the mantle is the convective upwelling of hot mantle parcels, but the horizontal scale of the convection cells is too small to account for the differences between the geochemical terranes (Michel et al., 2013; Tosi et al., 2013). A heterogeneous pattern of upwellings and a variable degree of total partial melt might result from an early inhomogeneous production of crustal units (O'Neill et al.,

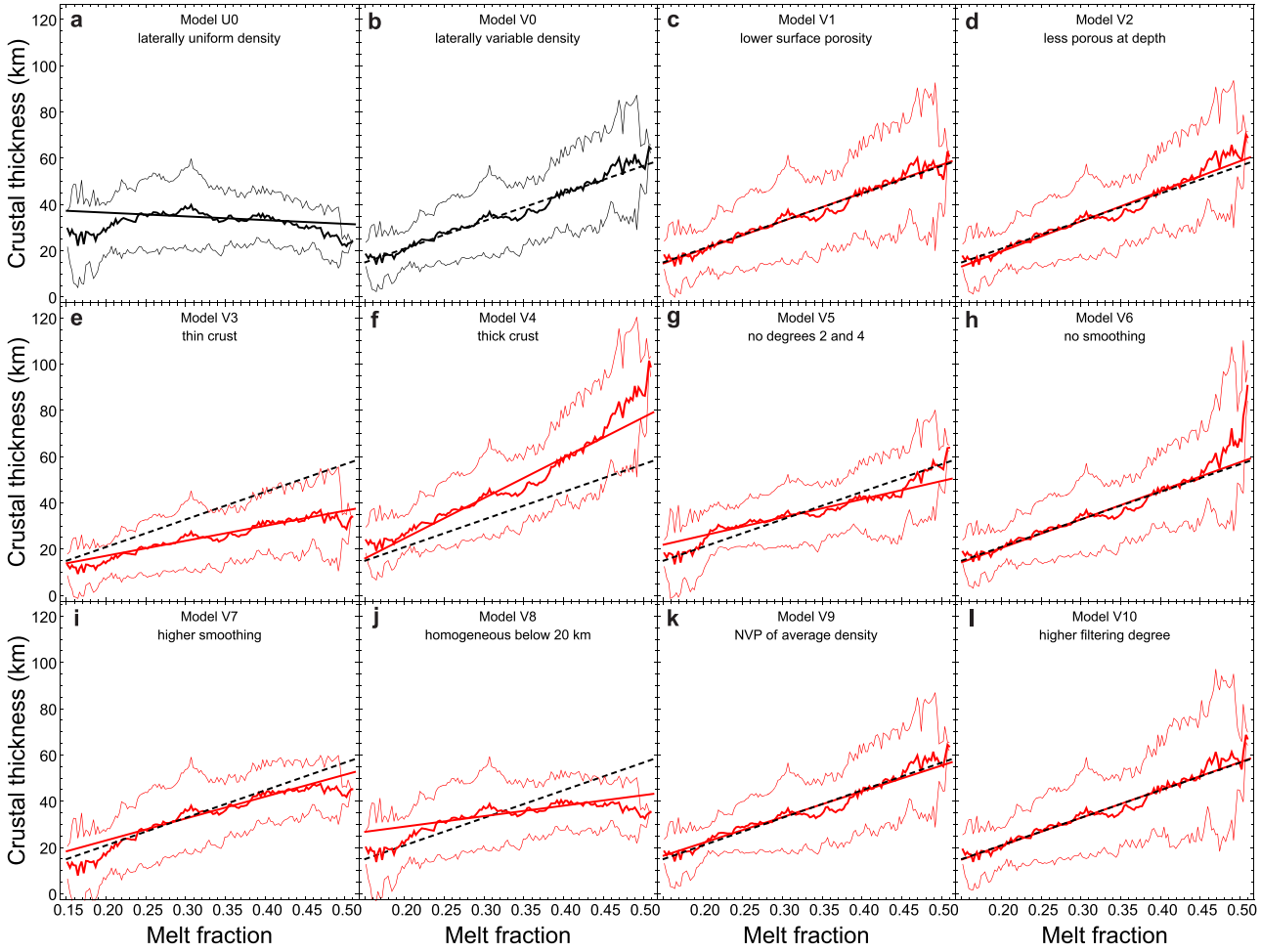

Figure 3. Crustal thickness as a function of the degree of mantle partial melting for the North Hemisphere of Mercury. Panels (a)–(l) show the 12 crustal thickness models of Table 1. In each panel, the middle thick curve shows the moving average of the scatter plot (equal-area grid), while the top and bottom curves delimit the 95% confidence level. Solid straight lines represent the least-squares linear fit. Dashed lines in panels (c)–(l) represent the linear fit for the reference Model V0 shown in panel (b). The width of melt fraction bins is equal to 0.0025.

2005), but this requirement is also in need of an explanation. Localized high melt fraction on Mercury might be triggered by impacts (Padovan et al., 2017; Roberts & Barnouin, 2012). Alternatively, some degree of heterogeneity of the mantle composition associated with a different melt productivity, possibly with variable clinopyroxene fraction due to differentiation produced by magma ocean solidification (Brown & Elkins-Tanton, 2009; Charlier et al., 2013; Namur et al., 2016), will also affect the melt productivity of a mantle source with potential implications for crustal thickness (Katz et al., 2003). These explanations are partly speculative; the origin of spatial variations in partial melting remains an open question.

Crustal thickness variations unrelated to variable melt fraction can have several causes. Although differentiation between the mantle and the secondary crust must be mainly driven by mantle melt extraction and surface emplacement, complex crustal formation processes and later modifications due to impacts and tectonics imply that the crust must be heterogeneous on small scales. At the longest wavelengths, part of crustal thickness variability might also be an artifact of the model if lateral density variations change significantly with depth. At shorter wavelengths, they could be due to a lack of resolution in the map of lateral density variations.

A link between crustal thickness and mantle melt production has also been identified on Earth in geodynamic settings with high production of mafic magma. For mid-ocean ridge basalts, geochemical proxies for temperature variations in the mantle correlate with crustal thickness in the range of 2 to 15 km (Asimow et al., 2001; Klein & Langmuir, 1987). The oceanic crust on Earth is also a typical example of secondary

crust produced similarly to that of Mercury: adiabatic decompression and partial melting of the mantle. There is also a large difference between the lower average thickness of the oceanic crust and thicker oceanic plateaus. This is commonly explained by mantle plumes being hotter than the surrounding mantle and leading to a higher degree of mantle melting responsible for the chemical and physical characteristics of oceanic plateaus (Kerr, 2014). On Mars, a link has been established between the density of erupted basalts forming the crust and the temperature conditions of partial melting in the mantle (Baratoux et al., 2014). A correlation between crustal thickness, the density of the crust, and melting conditions can thus be expected. The prime origin of these correlations is the thermal evolution of planetary interiors and particularly the cooling of the mantle over time (Baratoux et al., 2011; Namur et al., 2016; Padovan et al., 2017). Variations in surface composition are thus a unique record of secular cooling of the mantle during the early history of Mercury, a planet that became magmatically inactive by 3.5 Ga (Byrne et al., 2016). Overall, the correlation we observe at the planetary scale on Mercury between mantle melt production and the thickness of the crust might be a general feature of secondary magmatic crusts of terrestrial planets.

5. Conclusions

Geochemical mapping of Mercury by MESSENGER, in combination with laboratory measurements, can be confidently interpreted to yield the surface distributions of rock density and of the degree of mantle melting to form these rocks. Assuming that the composition of the crust does not change significantly with depth, we computed a new map of the crustal thickness and showed that the crust is thickest in the high-Mg terrane, previously thought to be an area of thinner crust. This result does not support an impact origin for this terrane. In addition, more than one half of crustal thickness variations in the Northern Hemisphere can be explained by lateral variations in mantle melting, suggesting that heterogeneous mantle melt led to the spatially variable build-up of the crust. The validity of the link between crustal thickness and mantle melt production will be tested in a few years by extending the analysis to the Southern Hemisphere when BepiColombo measurements become available. Whatever the conclusion, the maps of surface density and partial melting of surface rocks provided here will be useful for further investigations.

Acknowledgments
We thank Mike Sori for commenting on an earlier version of the paper. We are also grateful to Nicola Tosi and Peter James for their detailed reviews. X-ray spectrometer maps of Mercury are available on the Geosciences Node of the NASA Planetary Data System (https://pds-geosciences.wustl.edu/messenger/mess-h-xrs-3-rdr-maps-v1/messxrs_3001/data/maps/) and in the supporting information of Nittler et al. (2020). The gravity field HgM008 and the shape model GTMES 150v05 are also available on the Geosciences Node of the NASA Planetary Data System (https://pds-geosciences.wustl.edu/messenger/mess-h-rss_mla-5-sdp-v1/messrs_1001/data/shadr/). The maps of surface density, degree of mantle melting, and crustal thickness are available in a digital form on Zenodo (https://doi.org/10.5281/zenodo.3727115). This research has been supported by the BRAIN-be program (BR/143/A2/COME-IN) and the Belgian PRODEX program managed by the European Space Agency in collaboration with the Belgian Federal Science Policy Office. B. C. is a research associate of the Belgian Fund for Scientific Research-FNRS.

References

Asimow, P. D., Hirschmann, M. M., & Stolper, E. M. (2001). Calculation of peridotite partial melting from thermodynamic models of minerals and melts, IV. Adiabatic decompression and the composition and mean properties of mid-ocean ridge basalts. *Journal of Petrology*, *42*(5), 963–998. https://doi.org/10.1093/petrology/42.5.963

Baratoux, D., Samuel, H., Michaut, C., Toplis, M. J., Monnereau, M., Wieczorek, M., et al. (2014). Petrological constraints on the density of the Martian crust. *Journal of Geophysical Research: Planets*, *119*, 1707–1727. https://doi.org/10.1002/2014JE004642

Baratoux, D., Toplis, M. J., Monnereau, M., & Gasnault, O. (2011). Thermal history of Mars inferred from orbital geochemistry of volcanic provinces. *Nature*, *472*(7343), 338–341. https://doi.org/10.1038/nature09903

Besserer, J., Nimmo, F., Wieczorek, M. A., Weber, R. C., Kiefer, W. S., McGovern, P. J., et al. (2014). GRAIL gravity constraints on the vertical and lateral density structure of the lunar crust. *Geophysical Research Letters*, *41*, 5771–5777. https://doi.org/10.1002/2014GL060240

Brown, S. M., & Elkins-Tanton, L. T. (2009). Compositions of Mercury's earliest crust from magma ocean models. *Earth and Planetary Science Letters*, *286*(3-4), 446–455. https://doi.org/10.1016/j.epsl.2009.07.010

Byrne, P. K., Ostrach, L. R., Fassett, C. I., Chapman, C. R., Denevi, B. W., Evans, A. J., et al. (2016). Widespread effusive volcanism on Mercury likely ended by about 3.5 Ga. *Geophysical Research Letters*, *43*, 7408–7416. https://doi.org/10.1002/2016GL069412

Charlier, B., Grove, T. L., & Zuber, M. T. (2013). Phase equilibria of ultramafic compositions on Mercury and the origin of the compositional dichotomy. *Earth and Planetary Science Letters*, *363*, 50–60. https://doi.org/10.1016/j.epsl.2012.12.021

Denevi, B. W., Ernst, C. M., Meyer, H. M., Robinson, M. S., Murchie, S. L., Whitten, J. L., et al. (2013). The distribution and origin of smooth plains on Mercury. *Journal of Geophysical Research: Planets*, *118*, 891–907. https://doi.org/10.1002/jgre.20075

Fassett, C. I., Head, J. W., Baker, D. M. H., Zuber, M. T., Smith, D. E., Neumann, G. A., et al. (2012). Large impact basins on Mercury: Global distribution, characteristics, and modification history from MESSENGER orbital data. *Journal of Geophysical Research*, *117*, E00L08. https://doi.org/10.1029/2012JE004154

Frank, E. A., Potter, R. W. K., Abramov, O., James, P. B., Klima, R. L., Mojzsis, S. J., & Nittler, L. R. (2017). Evaluating an impact origin for Mercury's high-magnesium region. *Journal of Geophysical Research: Planets*, *122*, 614–632. https://doi.org/10.1002/2016JE005244

Genova, A., Goossens, S., Mazarico, E., Lemoine, F. G., Neumann, G. A., Kuang, W., et al. (2019). Geodetic evidence that Mercury has a solid inner core. *Geophysical Research Letters*, *46*, 3625–3633. https://doi.org/10.1029/2018GL081135

Goossens, S., Sabaka, T. J., Genova, A., Mazarico, E., Nicholas, J. B., & Neumann, G. A. (2017). Evidence for a low bulk crustal density for Mars from gravity and topography. *Geophysical Research Letters*, *44*, 7686–7694. https://doi.org/10.1002/2017GL074172

Han, S.-C., Schmerr, N., Neumann, G., & Holmes, S. (2014). Global characteristics of porosity and density stratification within the lunar crust from GRAIL gravity and Lunar Orbiter Laser Altimeter topography data. *Geophysical Research Letters*, *41*, 1882–1889. https://doi.org/10.1002/2014GL059378

Hauck, S. A., Margot, J.-L., Solomon, S. C., Phillips, R. J., Johnson, C. L., Lemoine, F. G., et al. (2013). The curious case of Mercury's internal structure. *Journal of Geophysical Research: Planets*, *118*, 1204–1220. https://doi.org/10.1002/jgre.20091

Head, J. W., Chapman, C. R., Strom, R. G., Fassett, C. I., Denevi, B. W., Blewett, D. T., et al. (2011). Flood volcanism in the northern high latitudes of Mercury revealed by MESSENGER. *Science*, *333*(6051), 1853. https://doi.org/10.1126/science.1211997

Head, J. W., Murchie, S. L., Prockter, L. M., Robinson, M. S., Solomon, S. C., Strom, R. G., et al. (2008). Volcanism on Mercury: Evidence from the first MESSENGER flyby. *Science*, *321*(5885), 69. https://doi.org/10.1126/science.1159256

Herzberg, C., & Gazel, E. (2009). Petrological evidence for secular cooling in mantle plumes. *Nature*, *458*(7238), 619–622. https://doi.org/10.1038/nature07857

Hirschmann, M. M. (2000). Mantle solidus: Experimental constraints and the effects of peridotite composition. *Geochemistry, Geophysics, Geosystems*, *1*(10), 1042–26. https://doi.org/10.1029/2000GC000070

James, P. B., Goossens, S., & Mazarico, E. (2019). Crustal density estimation from line-of-sight accelerations at mercury, 50th Lunar and Planetary Science Conference, The Woodlands, Texas, USA, abstract 2458. https://www.hou.usra.edu/meetings/lpsc2019/pdf/2458.pdf

James, P. B., Zuber, M. T., Phillips, R. J., & Solomon, S. C. (2015). Support of long-wavelength topography on Mercury inferred from MESSENGER measurements of gravity and topography. *Journal of Geophysical Research: Planets*, *120*, 287–310. https://doi.org/10.1002/2014JE004713

Katz, R. F., Spiegelman, M., & Langmuir, C. H. (2003). A new parameterization of hydrous mantle melting. *Geochemistry, Geophysics, Geosystems*, *4*(9), 1073. https://doi.org/10.1029/2002GC000433

Kerr, A. C. (2014). Oceanic plateaus, (2nd ed.). In H. D. Holland, & K. K. Turekian (Eds.), *Treatise on geochemistry* (pp. 631–667). Oxford: Elsevier.

Klein, E. M., & Langmuir, C. H. (1987). Global correlations of ocean ridge basalt chemistry with axial depth and crustal thickness. *Journal of Geophysical Research*, *92*(B8), 8089–8115. https://doi.org/10.1029/JB092iB08p08089

Konopliv, A. S., Park, R. S., & Ermakov, A. I. (2020). The Mercury gravity field, orientation, love number, and ephemeris from the MESSENGER radiometric tracking data. *Icarus*, *335*, 113,386. https://doi.org/10.1016/j.icarus.2019.07.020

Malavergne, V., Toplis, M. J., Berthet, S., & Jones, J. (2010). Highly reducing conditions during core formation on Mercury: Implications for internal structure and the origin of a magnetic field. *Icarus*, *206*(1), 199–209. https://doi.org/10.1016/j.icarus.2009.09.001

Marchi, S., Chapman, C. R., Fassett, C. I., Head, J. W., Bottke, W. F., & Strom, R. G. (2013). Global resurfacing of Mercury 4.0–4.1 billion years ago by heavy bombardment and volcanism. *Nature*, *499*(7456), 59–61. https://doi.org/10.1038/nature12280

Margot, J.-L., Hauck, S. A. II., Mazarico, E., Padovan, S., & Peale, S. J. (2018). Mercury's internal structure. In S. C. Solomon, L. R. Nittler, & B. J. Anderson (Eds.), *Mercury: The view after MESSENGER* (pp. 85–113). Cambridge: Cambridge University Press. https://doi.org/10.1017/9781316650684.005

Mazarico, E., Genova, A., Goossens, S., Lemoine, F. G., Neumann, G. A., Zuber, M. T., et al. (2014). The gravity field, orientation, and ephemeris of Mercury from MESSENGER observations after three years in orbit. *Journal of Geophysical Research: Planets*, *119*, 2417–2436. https://doi.org/10.1002/2014JE004675

Michel, N. C., Hauck, S. A., Solomon, S. C., Phillips, R. J., Roberts, J. H., & Zuber, M. T. (2013). Thermal evolution of Mercury as constrained by MESSENGER observations. *Journal of Geophysical Research: Planets*, *118*, 1033–1044. https://doi.org/10.1002/jgre.20049

Namur, O., & Charlier, B. (2017). Silicate mineralogy at the surface of Mercury. *Nature Geoscience*, *10*, 9–13. https://doi.org/10.1038/ngeo2860

Namur, O., Collinet, M., Charlier, B., Grove, T. L., Holtz, F., & McCammon, C. (2016). Melting processes and mantle sources of lavas on Mercury. *Earth and Planetary Science Letters*, *439*, 117–128. https://doi.org/10.1016/j.epsl.2016.01.030

Neumann, G. A., Perry, M. E., Mazarico, E., Ernst, C. M., Zuber, M. T., Smith, D. E., et al. (2016). Mercury shape model from laser altimetry and planetary comparisons, 47th Lunar and Planetary Science Conference, The Woodlands, Texas, USA, abstract 2087. Retrieved from https://www.hou.usra.edu/meetings/lpsc2016/pdf/2087.pdf

Nittler, L. R., Chabot, N. L., Grove, T. L., & Peplowski, P. N. (2018). The chemical composition of Mercury. In S. C. Solomon, L. R. Nittler, & B. J. Anderson (Eds.), *Mercury: The view after MESSENGER* (pp. 30–51). Cambridge: Cambridge University Press. https://doi.org/10.1017/9781316650684.003

Nittler, L. R., Frank, E. A., Weider, S. Z., Crapster-Pregont, E., Vorburger, A., Starr, R. D., & Solomon, S. C. (2020). Global major-element maps of Mercury from four years of MESSENGER X-ray spectrometer observations. *Icarus*, *345*, 113716. https://doi.org/10.1016/j.icarus.2020.113716

O'Neill, C., Moresi, L., & Lenardic, A. (2005). Insulation and depletion due to thickened crust: Effects on melt production on Mars and Earth. *Geophysical Research Letters*, *32*, L14304. https://doi.org/10.1029/2005GL022855

Padovan, S., Tosi, N., Plesa, A.-C., & Ruedas, T. (2017). Impact-induced changes in source depth and volume of magmatism on Mercury and their observational signatures. *Nature Communications*, *8*, 1945. https://doi.org/10.1038/s41467-017-01692-0

Padovan, S., Wieczorek, M. A., Margot, J.-L., Tosi, N., & Solomon, S. C. (2015). Thickness of the crust of Mercury from geoid-to-topography ratios. *Geophysical Research Letters*, *42*, 1029–1038. https://doi.org/10.1002/2014GL062487

Phillips, R. J., Byrne, P. K., James, P. B., Mazarico, E., Neumann, G. A., & Perry, M. E. (2018). Mercury's crust and lithosphere: Structure and mechanics. In S. C. Solomon, L. R. Nittler, & B. J. Anderson (Eds.), *Mercury: The view after MESSENGER* (pp. 52–84). Cambridge: Cambridge University Press. https://doi.org/10.1017/9781316650684.004

Rivoldini, A., & Van Hoolst, T. (2013). The interior structure of Mercury constrained by the low-degree gravity field and the rotation of Mercury. *Earth and Planetary Science Letters*, *377*, 62–72. https://doi.org/10.1016/j.epsl.2013.07.021

Roberts, J. H., & Barnouin, O. S. (2012). The effect of the Caloris impact on the mantle dynamics and volcanism of Mercury. *Journal of Geophysical Research*, *117*, E02007. https://doi.org/10.1029/2011JE003876

Sori, M. M. (2018). A thin, dense crust for Mercury. *Earth and Planetary Science Letters*, *489*, 92–99. https://doi.org/10.1016/j.epsl.2018.02.033

Stockstill-Cahill, K. R., McCoy, T. J., Nittler, L. R., Weider, S. Z., & Hauck, S. A. II (2012). Magnesium-rich crustal compositions on Mercury: Implications for magmatism from petrologic modeling. *Journal of Geophysical Research*, *117*, E00L15. https://doi.org/10.1029/2012JE004140

Tosi, N., Grott, M., Plesa, A. C., & Breuer, D. (2013). Thermochemical evolution of Mercury's interior. *Journal of Geophysical Research: Planets*, *118*, 2474–2487. https://doi.org/10.1002/jgre.20168

Tosi, N., & Padovan, S. (2020). Mercury, Moon, Mars: Surface expressions of mantle convection and interior evolution of stagnant-lid bodies. In H. Marquardt, M. Ballmer, S. Cottar, & K. Jasper (Eds.), *Mantle convection and surface expressions*, AGU Monograph Series. Washington, DC. https://arxiv.org/abs/1912.05207

Tosi, N., Čadek, O., Běhounková, M., Kánová, M., Plesa, A.-C., Grott, M., et al. (2015). Mercury's low-degree geoid and topography controlled by insolation-driven elastic deformation. *Geophysical Research Letters*, *42*, 7327–7335. https://doi.org/10.1002/2015GL065314

Vander Kaaden, K. E., McCubbin, F. M., Nittler, L. R., Peplowski, P. N., Weider, S. Z., Frank, E. A., & McCoy, T. J. (2017). Geochemistry, mineralogy, and petrology of boninitic and komatiitic rocks on the Mercurian surface: Insights into the Mercurian mantle. *Icarus*, *285*, 155–168. https://doi.org/10.1016/j.icarus.2016.11.041

Wasylenki, L. E., Baker, M. B., Kent, A. J. R., & Stolper, E. M. (2003). Near-solidus melting of the shallow upper mantle: Partial melting experiments on depleted peridotite. *Journal of Petrology*, *44*(7), 1163–1191. https://doi.org/10.1093/petrology/44.7.1163

Weider, S. Z., Nittler, L. R., Starr, R. D., Crapster-Pregont, E. J., Peplowski, P. N., Denevi, B. W., et al. (2015). Evidence for geochemical terranes on Mercury: Global mapping of major elements with MESSENGER's X-ray spectrometer. *Earth and Planetary Science Letters*, *416*, 109–120. https://doi.org/10.1016/j.epsl.2015.01.023

Wieczorek, M. A., Neumann, G. A., Nimmo, F., Kiefer, W. S., Taylor, G. J., Melosh, H. J., et al. (2013). The crust of the Moon as seen by GRAIL. *Science*, *339*, 671–675. https://doi.org/10.1126/science.1231530